Available online at www.sciencedirect.com
ScienceDirect
Journal of Nuclear Materials 372 (2008) 152–159
journal of nuclear materials
www.elsevier.com/locate/jnucmat

Breakaway phenomenon of Zr-based alloys during a high-temperature oxidation

Jong Hyuk Baek *, Yong Hwan Jeong

Advanced Core Materials Lab., Korea Atomic Energy Research Institute, P.O. Box 105, Yuseong, Daejeon 305-600, South Korea

Received 24 October 2006; accepted 26 February 2007

Abstract

The breakaway oxidation phenomena in Zr-based alloys were studied in the temperature range of 950–1200 °C for up to 36000 s by using a modified thermo-gravimetric analyzer. After the oxidation tests, the oxidation behaviors, breakaway oxidation time, hydrogen pick-up contents, and oxidation rate constants of the alloys were systematically evaluated in this study. The breakaway oxidation time was shortened with an increase of the Sn content in the Zr alloys. A breakaway oxidation phenomenon could be caused by the transition of a tetragonal oxide phase into a monoclinic one, and the oxide transition could lead to form the oxide cracks in both the lateral and radial directions. The cracks within the oxide layer could result in catastrophic increase in the weight gain rates and rapid increase the hydrogen pick-up within the oxygen-stabilized α-Zr and prior β-Zr layers. The oxidation rate constants calculated from the post-breakaway data in the Zr alloys with breakaway oxidation behaviors matched well with the values from both the Baker–Just and Cathcart–Pawel correlations.

PACS: 42.81.B; 81.65.M; 81.65.K

1. Introduction

The structural integrity of a fuel cladding under normal and abnormal operation conditions should be considered to secure its safety in the design of a light water reactor. The design based specific accidents, such as a LOCA (Loss of coolant accident) and RIA (Reactivity initiated accident), should be evaluated to guarantee the mechanical integrity of a fuel cladding. In the high burn-up fuel, especially, the safety-related criteria, including the LOCA and RIA, have become a key issue in the nuclear fuel research fields. Because a fuel is a primary source of radioactivity and heat generation in a nuclear reactor, such a criterion is usually established on the basis of the characteristics of a fuel cladding under specific accident situations.

During a typical LOCA condition, the cladding is subjected to a high-temperature oxidation which is finally quenched because of an emergency coolant reflooding into the reactor core. In this LOCA situation, the equivalent cladding reacted (ECR) should not exceed the criterion of 17% and the peak cladding temperature (PCT) should also be below 1200 °C [1]. The current trend for a nuclear fuel is to increase its discharge burn-up and cycle length because of the major advantages for a fuel cycle cost and spent fuel management. Several fuel vendors have developed advanced claddings, such as ZIRLO, M5, MDA, NDA, and HANA for the high burn-up fuel [2–8]. LOCA should be taken into account within the licensing procedures of the new developed Zr alloys for their application to a commercial reactor cladding [9]. Because the defects produced by an irradiation within the Zr matrix during a normal operation are regarded to anneal out rapidly at the beta phase temperatures in the process of a LOCA-like temperature oxidation, fortunately, the as-received cladding materials have usually been simulated in most LOCA tests [10–12].

LOCA performance of the advanced Zr-based claddings has been investigated actively [9–20]. Portier et al. [12] had

* Corresponding author. Tel.: +82 42 868 8823; fax: +82 42 862 0432.
E-mail address: jhbaek@kaeri.re.kr (J.H. Baek).

0022-3115/$ - see front matter © 2007 Elsevier B.V. All rights reserved.
doi:10.1016/j.jnucmat.2007.02.011

reported a breakaway oxidation, in which a sudden or 'catastrophic' increase of the oxidation rate was observed, in the Zircaloy-4 and M5 claddings when they were steam-oxidized for longer periods of more than 5000 s at 1000 °C. They reported that the oxidation kinetics of the claddings was transited from a parabolic rate to a quasi-linear rate at 1000 °C after 5000 s. Russian Zr-alloys (E110 and E635) have been reported to be susceptible to a breakaway oxidation and a premature embrittlement under LOCA-like conditions, even though the oxidation environment was steam which contained a negligible amount of H gas [13–18]. In contrast to the Russian alloys, the M5 alloy has been reported to be resistant to a breakaway oxidation under a similar condition [19]. And the ZIRLO results indicated a behavior similar to that of M5 [20]. That is, a susceptibility to a high-temperature breakaway oxidation is the key to understanding the contrasting performance of the Russian alloys (E110, E635) and Western alloys (M5, ZIRLO). Chung reported that the premature breakaway of the Russian alloys could have resulted from an excessive hydrogen pick-up due to different fabrication routes from the raw materials to the final tube [21]. The Ca, Mg, Al, Nb, and F could affect the high-temperature breakaway oxidation performance of the Zr alloys. Up to now, the validity of a breakaway oxidation at the LOCA-like temperatures remains to be confirmed by systematical studies. The breakaway oxidation phenomenon of advanced Zr alloys was investigated at LOCA-like temperatures in this study.

2. Experimental

The chemical composition of the Zr-based alloys used in this study is given in Table 1. Four (4) cladding-type samples and three (3) sheet-type ones were cut into 8 mm in length and $8 \times 8 \times 1$ mm^3 in cubic, respectively. Before the oxidation tests, the specimens were ground carefully up to Grit No. 1200 of SiC paper. Then all the specimens were pickled in a solution of 5% HF, 45% HNO_3, and 50% H_2O and cleaned ultrasonically in an ethanol and acetone solution. The oxidation tests in steam were conducted by using the apparatus already described in a previous paper [22]. The steam supply rate was 0.6 g/cm^2-min at standard temperature and pressure (STP). The test temperature ranged from 950 to 1200 °C and the duration was from 600 to 36000 s. The temperature gradient along the specimen length was less than 5 °C. The weight gains were determined by an in situ method within 0.001 mg with accuracy. After the oxidation tests, the hydrogen pick-up content was determined by a vacuum hot extraction method and the oxidation rate constants were also calculated on the basis of the parabolic rate law. An extrapolation method was applied to determine objectively the onset time of a breakaway oxidation at the transition point of the oxidation kinetics.

Table 1
Chemical composition of Zr-based alloys

ID	Nb	Sn	Fe	Cr	Cu	Zr	Remarks (wt%)
Z4	–	1.38	0.2	0.1	–	Bal.	Tube
ZL	1.0	1.0	0.1	–	–	Bal.	Tube
H4	1.5	0.4	0.2	0.1	–	Bal.	Tube
H5	0.4	0.8	0.35	0.15	0.1	Bal.	Tube
Zr–0.7%Sn	–	0.7	–	–	–	Bal.	Sheet
Zr–2.0%Sn	–	2.0	–	–	–	Bal.	Sheet
Zr–1.6%Nb	1.6	–	–	–	–	Bal.	Sheet

3. Results and discussion

Fig. 1 presents the oxidation behaviors of the tube-type specimens (Z4, ZL, H4 and H5) for the steam oxidation experiments performed at 1000 °C. In Fig. 1(a), the oxidation kinetics for an exposure time of less than 600 s obeyed the parabolic rate law, which is generally accepted for a high-temperature oxidation of Zr alloys under a steam atmosphere at that temperature. Although all the tube-type specimens were controlled by the parabolic rate law, the weight gains after an exposure for 600 s were different due to the variations of the alloying composition. The H4 alloy had the lowest weight gain when compared with the other alloys (Z4, ZL and H5). It was anticipated that the composition which was comprised of a high Nb (1.5%)

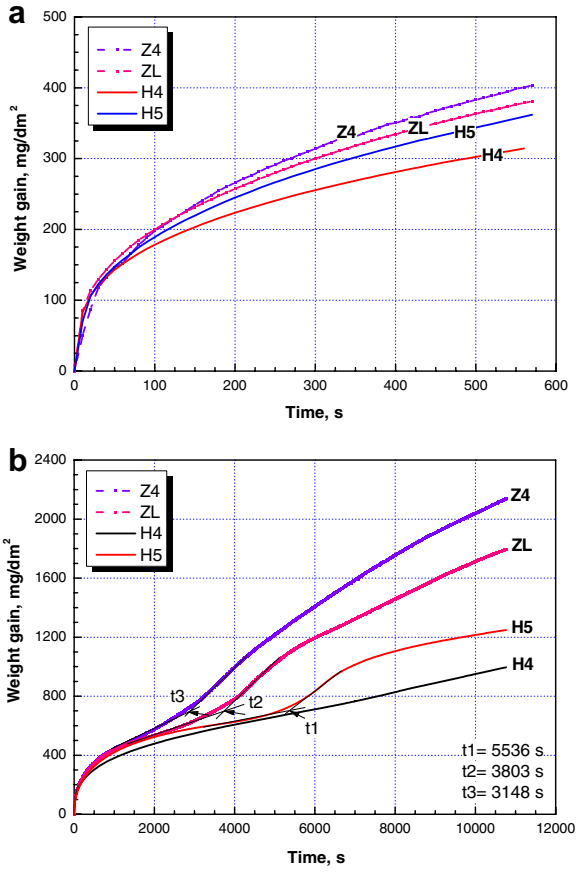

Fig. 1. Oxidation behaviors of Zr-based alloys at 1000 °C for (a) short-term (600 s) and (b) long-term (10800 s) periods.

and low Sn (0.4%) content for the H4 alloy would have an advantage of an oxidation resistance under the test condition.

The long-term oxidation behaviors of the tube-type specimens are shown in Fig. 1(b). The weight gain of the H4 alloy increased monotonously as the exposure time was extended to 10 800 s. No breakaway oxidation behavior in the H4 alloy was detected up to the exposure time at 1000 °C. However, the breakaway oxidation behaviors at the same temperature were observed in the Z4, ZL and H5 alloys. The breakaway oxidation of the H5 alloy occurred after an exposure for about 5500 s, the ZL alloy was about 3800 s, and the Z4 alloy was about 3100 s. It is possible to suppose that the breakaway oxidation kinetics would be influenced by the chemical composition of the Zr alloys.

According to a previous study [23], the breakaway time of the Zircaloy-4 was detected after a test for about 2400 s, which is shorter than our result, at the same oxidation temperature of 1000 °C. And another study reported that the breakaway time of the same compositional alloy was about 5000 s [12], which was a longer time than our result, and the breakaway oxidation time of the M5 and Zircaloy-4 alloys was the same in spite of the different alloying compositions [12]. Although the sample sizes in the previous studies were different from present one, a possible reason for these inconsistent breakaway onsets in Zircaloy-4 among the studies could be because of the differences in the measuring methods of the weight gain. The in situ measuring method used in the present study was to determine the weight gain during an oxidation. Meanwhile, the discrete measuring method was applied in other studies [12,23] after an oxidation. But it was difficult to understand fully why the breakaway onsets of the M5 and Zircaloy-4 alloys were almost the same in a previous study [12] although the oxidation rate and the hydrogen content in the two alloys had some differences after a breakaway time of about 5000 s.

In order to confirm the breakaway oxidation time of the Zr-based alloys, steam oxidation tests were carried out at 1000 °C for various exposures up to 10 800 s. Fig. 2 shows the examples of the test results for the Z4 and H4 alloys. The breakaway oxidation time of the Z4 alloys was almost the same from the repeatedly performed tests for the various exposures. But the H4 alloys did not show a breakaway oxidation behavior in spite of the different exposures. From these tests, the reproducibility of the breakaway oxidations can be ascertained in the present Z4, ZL and H5 alloys.

At a glance, from Fig. 1(b), it was anticipated that the breakaway time could be related to the chemical composition of the Zr alloys. The main difference in the chemical composition of the Z4, ZL, H4 and H5 alloys would be Sn and Nb. Regarding the Nb content, a breakaway oxidation occurred at about 3800 s in the ZL alloy (1.0% Nb) while it was not observed in the H4 alloy (1.5% Nb). Furthermore, the breakaway oxidation time was about 5500 s in the H5 alloy (0.4% Nb). The onset time of the breakaway oxidation could not be correlated with the Nb content in the Zr alloys. It was anticipated that the Nb content in the Zr alloys would be independent of the breakaway phenomenon during a steam oxidation.

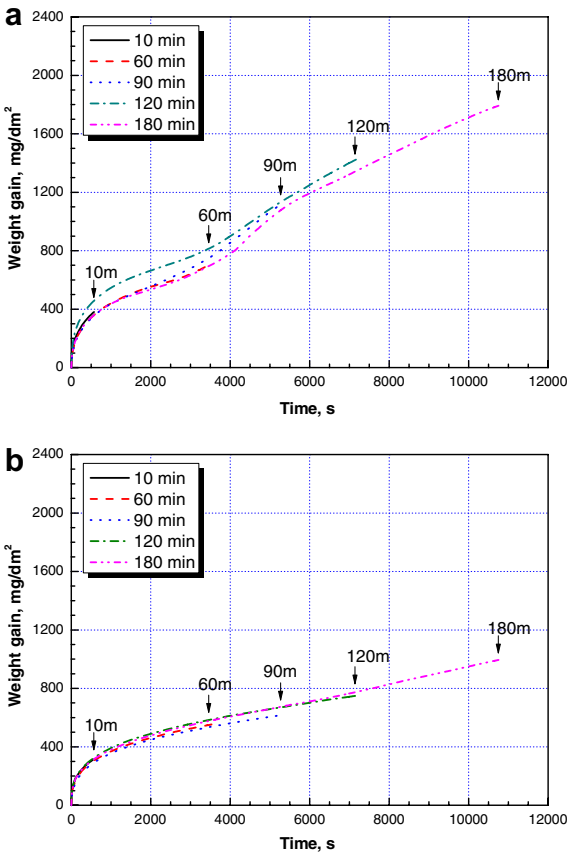

Fig. 2. Oxidation behaviors of (a) Z4 and (b) H4 alloys in 1000 °C steam.

The Z4, ZL and H5 alloys presented breakaway behaviors during a steam oxidation at 1000 °C. The Sn in the alloys ranged from 0.8% to 1.38%. Fig. 3 shows that the breakaway oxidation time with an variation of the Sn content in the alloys. The breakaway oxidation occurred for an earlier exposure time with an increasing Sn content within the alloys. It was thought that the Sn content could affect

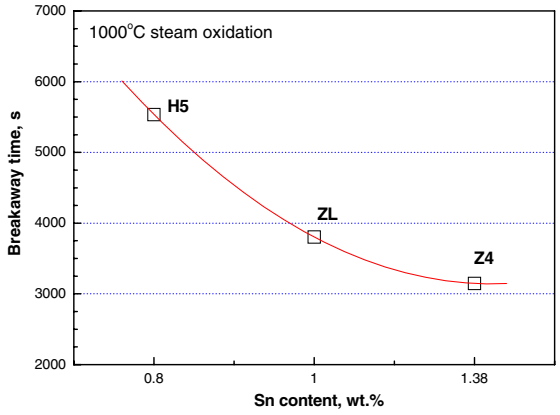

Fig. 3. Breakaway oxidation time of Z4, ZL and H5 alloys at 1000 °C.

the breakaway oxidation of the Zr alloys at 1000 °C. The Sn content of the Zr-based alloys would deteriorate the oxidation resistance at 1000 °C because of a premature breakaway oxidation.

The Sn content would affect the breakaway oxidation behaviors of Zr alloys at 1000 °C while the Nb content could not explain the behaviors. But the effects of the Sn and Nb contents on a breakaway oxidation in specific Zr–Sn or Zr–Nb binary alloys have not been reported up to now. A simple oxidation test was performed for the sheet-type Zr–0.7%Sn, Zr–2.0%Sn, and Zr–1.6%Nb alloys in this study so as to verify the Sn and Nb content effects on a breakaway oxidation of the binary Zr alloys, and the test results are presented in Fig. 4. The breakaway oxidation behavior was detected in the Zr–0.7%Sn and Zr–2.0%Sn alloys. But it did not appear in the Zr–1.6%Nb alloy for the tested exposure of 10 800 s. In addition, the breakaway time of the Zr–0.7%Sn alloy was about 6800 s and the Zr–2.0%Sn alloy was about 1700 s. As the Sn content in the sheet-type Zr–*x*Sn alloys increased, the breakaway time of the Zr alloys also decreased. This was the same trend for the tube-type specimens of the Z4, ZL and H5 alloys. The Sn content within the Zr-based alloys could influence the breakaway oxidation behavior and the breakaway time would be shortened with an increase of the Sn content within the alloys.

Fig. 5 shows the hydrogen content of the sheet-type Zr–0.7%Sn, Zr–2.0%Sn, and Zr–1.6%Nb alloys after the oxidation tests for 10 800 s. The hydrogen content of the Zr–2.0%Sn alloy was much higher than that of the Zr–0.7%Sn and Zr–1.6%Nb alloys. It was thought that the hydrogen ingress was raised sharply due to a rapid increase of the weight gains of the Zr–2.0%Sn alloy after the breakaway point at about 1700 s. It was anticipated that the hydrogen pick-up content during the steam oxidation would be influenced by the breakaway oxidation.

Returning to the oxidation of the tube-type specimens (Z4, ZL, H4 and H5 alloys), the hydrogen content of the alloys was also determined after the 1000 °C oxidation for 600–10 800 s. Fig. 6 shows the hydrogen pick-up content of the alloys as a function of the exposure time at 1000 °C. It is clearly seen that the hydrogen pick-up content of the alloys increased with an increase of the exposure time. In the case of the Z4 and ZL alloys, the hydrogen pick-up contents increased more rapidly than the H4 and H5 alloys due to a premature breakaway oxidation. But the hydrogen pick-up rate (i.e., slop in Fig. 6) of the H5 alloy was faster than the H4 alloy. It was anticipated that the hydrogen pick-up content was directly related to the weight gain during an oxidation process. So, it was interpreted that the higher weight gains could produce higher hydrogen pick-up content, as shown in Fig. 7. The hydrogen pick-up rate (i.e., slop in Fig. 7) in the Z4 and ZL alloys was larger than that of the H5 and H4 alloys. The premature breakaway oxidation of the Z4 and ZL alloys would be closely related to their larger hydrogen pick-up rate.

In Fig. 7, the relationship between the hydrogen pick-up content and the weight gain was expressed with a linearity when the weight gain was less than 1300 mg/dm^2. The hydrogen pick-up rate of the Z4 and ZL alloys was reduced in a range with a weight gain of more than 1300 mg/dm^2. This could be resulted from the thickness reduction of the oxygen-stabilized α-Zr and prior β-Zr layers. Generally, the hydrogen pick-up contents would increase with

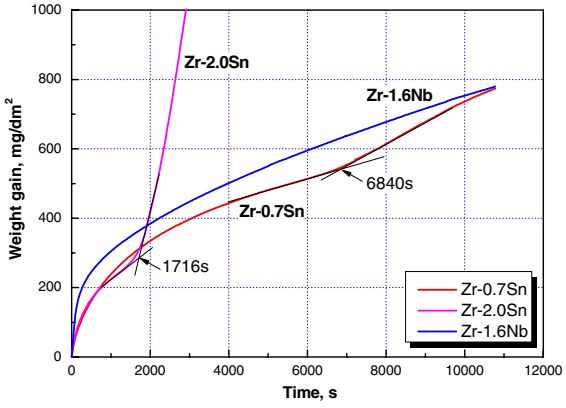

Fig. 4. Oxidation behaviors of Zr–0.7Sn, Zr–2.0Sn, and Zr–1.6Nb binary alloys at 1000 °C for 10 800 s.

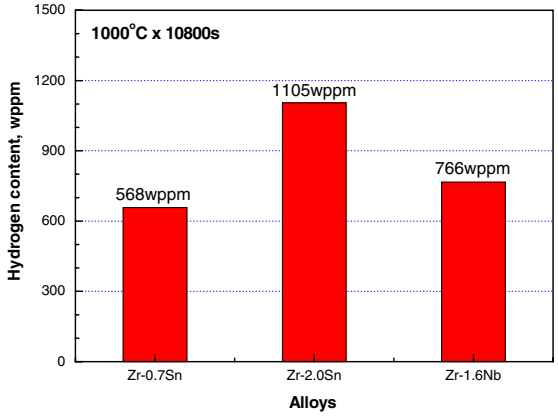

Fig. 5. Hydrogen content of Zr–0.7Sn, Zr–2.0Sn, and Zr–1.6Nb binary alloys after the oxidation at 1000 °C for 10 800 s.

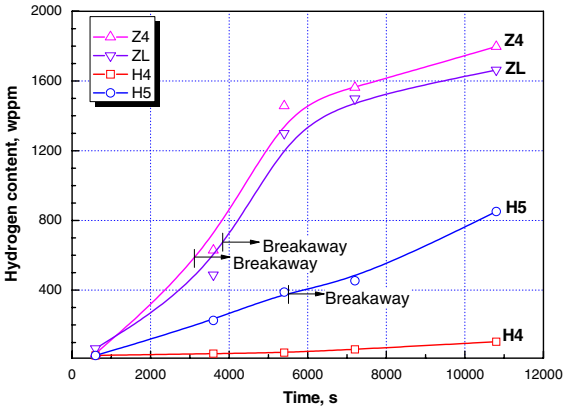

Fig. 6. Hydrogen pick-up contents during the steam oxidation at 1000 °C.

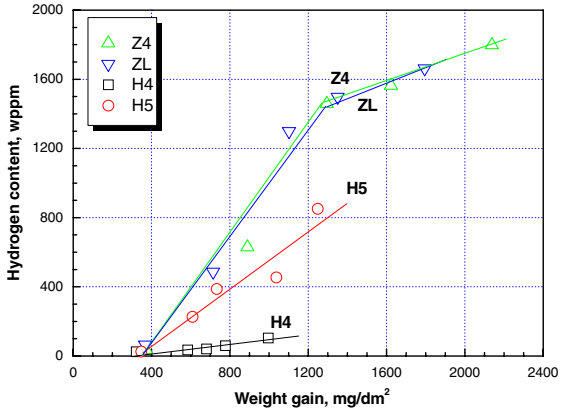

Fig. 7. Relationship between hydrogen pick-up contents and weight gains during the steam oxidation at 1000 °C.

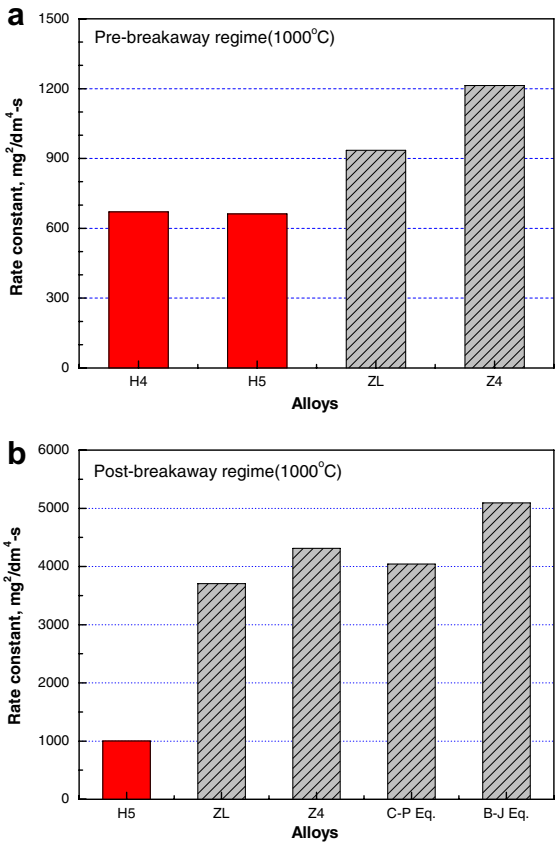

Fig. 8. Oxidation rate constant of 1000 °C steam reaction in (a) pre-breakaway and (b) post-breakaway regimes.

an increase of the weight gain during a high-temperature steam oxidation. At an early stage of an oxidation, the absorbed hydrogen would exist within both the oxygen-stabilized α-Zr layer and the prior β-Zr layer, not within the oxide layer. As the oxidation reaction was progressed sufficiently enough after the breakaway transition, the thickness of the oxygen-stabilized α-Zr and prior β-Zr layers would be reduced by the sudden increase of the oxide layer. The reduction of the both the oxygen-stabilized α-Zr and prior β-Zr layers was reported in a previous study [23]. The considerable reduction of both oxygen-stabilized α-Zr and prior β-Zr layers could decrease the hydrogen pick-up rate during the oxidation process. This could result in a reduction of the hydrogen pick-up rates in specimens with a sufficiently higher weigh gain.

The weight gains measured in the present study could be evaluated by assuming a parabolic rate law [24,25]. The parabolic oxidation rate constants of the tube-type Z4, ZL, H4, and H5 alloys were calculated from the data in Fig. 1, and presented in Fig. 8. In the pre-breakaway regime, the oxidation rate constants of the H4 and H5 alloys were lower than those of the Z4 and ZL alloys. At the post-breakaway regime, meanwhile, the oxidation rate constant of the H5 alloy was much lower than that of the Z4 and ZL alloys. The oxidation rate constants of the Z4 and ZL alloys from the this study agreed comparatively well with those from both the Baker–Just and Cathcart–Pawel correlations [24,25]. It was interpreted that the oxidation rate constants of the Zr-based alloys would be more appropriate to calculate the oxidation results at a post-breakaway regime rather than at a pre-breakaway regime. Compared with the Z4 and ZL alloys, the relatively lower rate constant of the H5 alloy at the post-breakaway regime would have resulted from the difference of their chemical composition.

For the Z4 and H4 alloys, the steam oxidation tests were performed to obtain the rate constants in the temperature range of 950–1200 °C. The Z4 alloy of Fig. 9(a) showed a transition of the oxidation kinetics in the temperature range from 950 to 1050 °C. In the case of the H4 alloy shown in Fig. 9(b), however, a transition of the oxidation kinetics did not occur at all the temperatures during the tested exposures. The different behaviors between the Z4 and H4 alloys could be explained by the chemical composition of the alloys. It is well-known that the Sn content within a Zr-based alloy could play a role in stabilizing the α-Zr phase and the Nb in stabilizing the β-Zr one [26,27]. Incidentally, the Sn content in the Z4 alloy was higher than that within the H4 alloy but Nb was not included in the alloy. It was expected that a phase transformation from the α + β phases to the β phase in the alloy would occur in the tested temperature range. It was thought that the transition of the oxidation kinetics in the Z4 alloy would be detected at the temperatures of 950–1050 °C. Furthermore, the Nb content in the Zr-based alloy could lower the formation temperature of the tetragonal ZrO_2 phase. Thus, the Nb addition in the H4 alloy could lower the transformation temperature of tetragonal ZrO_2 phase to monoclinic ZrO_2 one and then retain a relatively more stable phase of the tetragonal ZrO_2 for a prolonged exposure. This could also affect the hydrogen pick-up content during a steam oxidation.

The breakaway time was determined for the Z4 alloy at temperatures of 950–1050 °C and shown in Fig. 10. As the oxidation temperature increased, the breakaway oxidation time of the alloy was dramatically shortened up to 3800 s at 1000 °C. The breakaway time at 1050 °C was almost simi-

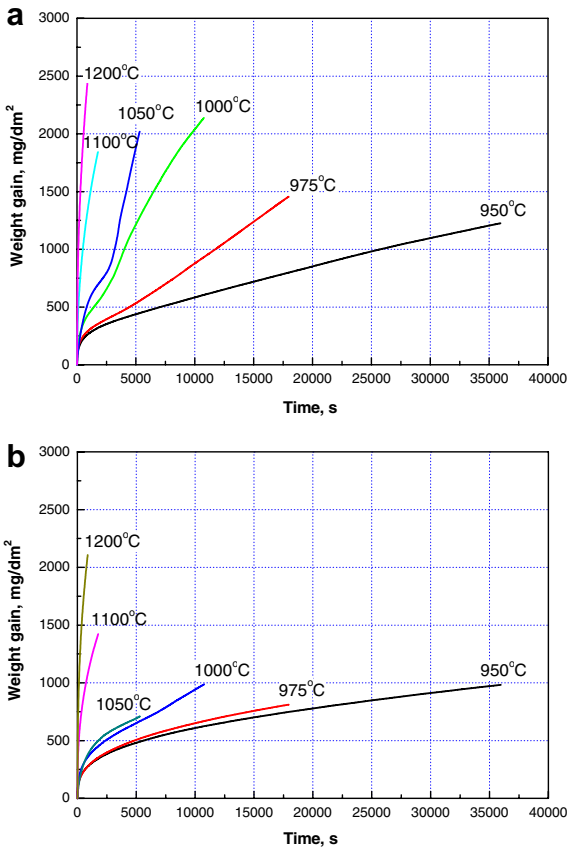

Fig. 9. Oxidation behaviors of (a) Z4 and (b) H4 alloys at 950–1200 °C temperatures.

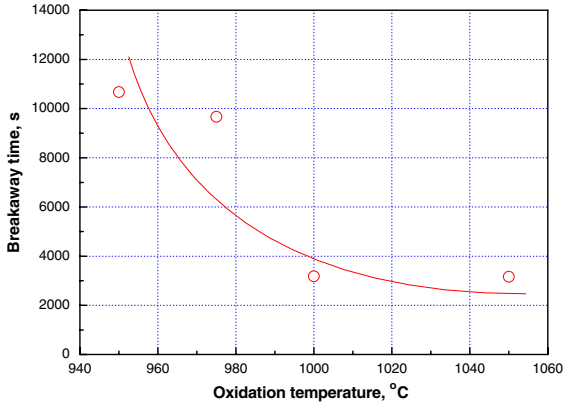

Fig. 10. Breakaway oxidation time of Z4 alloy at 950–1200 °C.

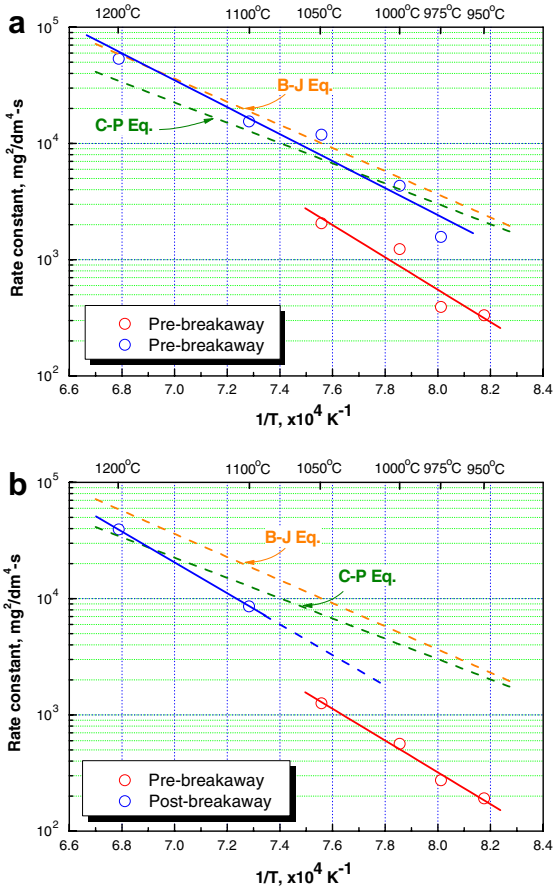

Fig. 11. Oxidation rate constants of (a) Z4 and (b) H4 alloys.

lar to that at 1000 °C. This means that the transformations of the metal and oxide (i.e., Zr matrix and ZrO_2) of the Z4 alloy actively happened in the temperature range.

The oxidation rate constants for the Z4 and H4 alloys were calculated in the pre-breakaway and post-breakaway oxidation regimes, respectively, and described in Fig. 11 together with the those from both the Baker–Just and Cathcart–Pawel correlations. The oxidation rate constants at the post-breakaway regime for the Z4 alloy nearly agreed with those from both the Baker–Just and Cathcart–Pawel correlations [24,25]. But the oxidation rate constants of two alloys at the pre-breakaway regime were lower than those by the two correlations. The oxidation rate constants of the Zr alloys for a LOCA prototypical exposure time of less than 1800 s between 950 and 1200 °C, in which the oxidation kinetics of the alloy was parabolic, would be more proper to analyze the data at the post-breakaway regime than at the pre-breakaway regime. The oxidation rate constants of the Z4 alloy were strongly dependent on the breakaway oxidation kinetics. Although the breakaway oxidation behaviors in the H4 alloy were not observed in the temperature range from 950 to 1050 °C, the oxidation rate constants at those temperatures were different from those at 1050–1100 °C. The oxidation rate constants of the H4 alloy between 1100 and 1200 °C lay on a straight line in the rate constant versus reciprocal temperature plot while those between 950 and 1050 °C were another straight line in the same plot.

The difference in the oxidation rate constants of the H4 alloy between the two temperature ranges could be understood from the viewpoint of the oxidation kinetics. It was thought that the oxidation rate would be faster above 1100 °C. Though the oxidation rate constants in the H4 alloy were sharply enhanced at above 1100 °C, the hydrogen pick-up content did not increase in the comparison with those of the Z4 alloy under the same oxidation condition.

From Fig. 11, the parabolic rate constants of the Zr-based alloys should be considered by using the oxidation results from the post-breakaway regime if the breakaway oxidation behaviors could be observed in the alloys in spite of a less than 1050 °C.

As a result of this study, it was summarized that the Sn addition in the Zr alloys could show the breakaway oxidation kinetics during the steam oxidation at temperatures of 950–1000 °C and the breakaway oxidation time could be shortened with an increase of the Sn contents within the alloys. The destabilization of the tetragonal oxide phase due to the higher Sn content was not reported during the oxidation at those temperatures. But, the addition of higher Sn in the Zr alloys would decrease the corrosion resistance at the temperatures of 350–400 °C [5,26]. By increasing the Sn content in the Zr alloys, the amount of the segregation Sn that ends up at the crystalline boundaries in the tetragonal phase oxide increased. The volume expansion form the oxidation increased with the oxidation of the greater amount of segregated Sn. Thus, the oxide transition from the tetragonal phase to the monoclinic one increases and the corrosion resistance was degraded. At LOCA-like temperatures, the Sn segregation in the oxide layer was generally reported in several studies [28–30]. From these reasons, the Sn segregation would occur within the oxide layer and then the Sn segregation could destabilize the tetragonal oxide phase in the higher Sn-contained alloys.

A destabilization of the tetragonal phase due to Sn segregation in an oxide layer could cause a lateral cracking and then a radial cracking within an oxide layer, as reported in a study [31]. The cracking in the oxide layer could also initiate breakaway oxidation behaviors because of the transition of the oxide phase [32,33]. The increase of the Sn content in the Zr alloys could enhance the oxide transformation and the breakaway oxidation time could be shortened with an increase of the Sn content within the alloys. At temperatures of 950–1200 °C under consideration two crystallographic modifications of an oxide phase are known, the tetragonal phase at higher temperatures and the monoclinic phase at lower temperatures [34,35]. Following Pemsler's assumption [33], it was concluded that the steam oxidation at 950–1050 °C, where the breakaway oxidations occurred in the Z4 alloy, would initially lead to a tetragonal oxide which is stabilized by a compressive stress and a high substoichiometry (ZrO_{2-x}). During a continued oxidation, a stress relaxation by the lateral and radial cracks within the oxide layer would destabilize the tendencies for a tetragonal oxide. The cracks within the oxide layer could enhance the oxygen and hydrogen movements through the oxide layer during a steam oxidation. Thus, the loss of the oxide protectiveness and the enhancement of the oxygen and hydrogen ingresses due to a breakaway oxidation would lead to the catastrophic increase of the oxidation kinetics.

Contrary to Sn, the Nb addition in the Zr alloys could promote a stabilization of the tetragonal ZrO_2 phase during a steam oxidation. The Nb in the Zr-based alloy could help sustain a tetragonal oxide phase for much longer exposure periods. When the Nb addition was about 1.5%, such as in the H4 alloy, breakaway oxidation behaviors could be restrained in that alloy. It was thought that the resistance to the breakaway oxidation could be promoted by the higher Nb addition (~1.5%) into the Zr-based alloys. In addition, the hydrogen pick-up could be also reduced by the higher Nb addition.

The different composition in the Zr alloys would affect simultaneously both the breakaway oxidation kinetics and the oxide phase transition. I thought that this hypothesis could be applied to explain the breakaway oxidation kinetics in the different compositional alloys. The tetragonal-to-monoclinic transition was an instability that initiated at local regions of the metal–oxide interface and grew rapidly throughout the oxide layer. This oxide transition would result in an increase in oxidation rate. Along with this increase in oxidation rate due to cracks in the monoclinic oxide layer, there would be significant weigh gains due to the path-shortening of oxygen and hydrogen movements through the cracks.

Recently, the Russian cladding (E110) test program had been carried out to determine why the cladding exhibited such short breakaway oxidation times (approximately 600 s at 1000 °C) as compared to the breakaway oxidation times (>6000 s at 1000 °C) for the Zr–1Nb cladding (M5) used in the States [36]. The differences in surface roughness along with possible differences in surface impurities were considered as plausible reasons for the behavior differences. It was concluded that the combination of higher-surface roughness and etching with HF containing acid mixtures could promote the monoclinic-oxide formation, which could reduce breakaway oxidation time [36]. In this point of view, the breakaway oxidation kinetics could be interpreted by the oxide transition from the tetragonal phase to monoclinic one.

The hydrogen content in the oxygen-stabilized α-Zr and prior β-Zr phase layers could enhance the oxygen absorption in its layer [37]. That is, an increase of the hydrogen pick-up into both layers could increase the weight gain during a steam oxidation because of an enhancement of the oxygen solubility within the layers [37], and cause the breakaway oxidation kinetics in the higher Sn-containing Zr alloys. Zr alloys containing a lower Sn content and a higher Nb content would be more effective in maintaining the tetragonal oxide phase for longer exposures.

In the Z4 alloy in this study, the calculated rate constants from the post-breakaway data were well correlated with the values from both the Baker–Just and Cathcart–Pawel correlations. Therefore, the rate constants of Zr alloys should be calculated with a consideration of the breakaway oxidation phenomena.

4. Conclusions

The oxidation experiments of Zr-based alloys (Z4, ZL, H4, and H5) under a steam atmosphere at 950–1200 °C

for up to 36 000 s showed breakaway oxidation behaviors in the higher Sn-containing Zr alloys. The breakaway oxidation time was shortened with an increase of the Sn content within the Zr alloys because of a destabilization effect of the tetragonal oxide layer and a cracking within the oxide layer by the Sn addition. A breakaway oxidation could be postulated by the oxide transition from tetragonal phase into monoclinic one and by an oxide cracking in both the lateral and radial directions. And the crack formation could shorten the movement path of the oxygen and hydrogen through the oxide layer, and then a catastrophic increase in the weight gain rates could be presented as breakaway oxidation kinetics. The oxidation rate constants calculated from the post-breakaway data in the Zr-based alloys with a breakaway oxidation behavior matched well with the values from both the Baker–Just and Cathcart–Pawel correlations. It was concluded that the oxidation rate constants should be calculated with a consideration of the breakaway behaviors when the breakaway oxidation kinetics has occurred during a steam oxidation at 950–1200 °C.

Acknowledgements

This study was supported by Korea Science and Engineering Foundation (KOSEF) and Ministry of Science and Technology (MOST), Korean government, through its National Nuclear Technology Program.

References

[1] USNRC-SRP (Standard Review Plan), Sec. 4.2, NUREG-0800.
[2] G.P. Sabol, R.J. Comstock, R.A. Weiner, P. Larouere, R.N. Stanutz, in: Zirconium in the Nuclear Industry: Tenth International Symposium, ASTM STP 1245, 1994, p. 724.
[3] J.-P. Mardon, D. Charquet, J. Senevat, in: Zirconium in the Nuclear Industry: Twelfth International Symposium, ASTM STP 1354, 2000, p. 505.
[4] T. Isobe, Y. Matsuo, in: Zirconium in the Nuclear Industry: Ninth International Symposium, ASTM STP 1132, 1991, p. 346.
[5] T. Harada, M. Kimpara, K. Abe, in: Zirconium in the Nuclear Industry: Ninth International Symposium, ASTM STP 1132, 1991, p. 368.
[6] Y. Etoh, S. Shimada, T. Yasuda, T. Ikeda, R.B. Adamson, J.-S. Fred Chen, Y. Ishii, K. Takai, in: Zirconium in the Nuclear Industry: Eleventh International Symposium, ASTM STP 1295, 1996, p. 825.
[7] Y.H. Jeong, S.Y. Park, M.H. Lee, B.K. Choi, J.H. Baek, J.Y. Park, J.H. Kim, H.G. Kim, J. Nucl. Sci. Technol. 43 (9) (2006) 997.
[8] Y.H. Jeong, J.H. Baek, J.Y. Park, in: Proceedings of IAEA Technical Meeting on Corrosion Resistance Zirconium Alloys, Buenos Aires, Argentina, 2005.
[9] F.J. Erbacher, S. Leistikow, in: Zirconium in the Nuclear Industry: Seventh International Symposium, ASTM STP 939, 1987, p. 451.
[10] M. Ozawa, T. Takahashi, T. Homma, K. Goto, in: Zirconium in the Nuclear Industry: Twelfth International Symposium, ASTM STP 1354, 2000, p. 279.
[11] M. Aomi, N. Nakatsuka, S. Komura, T. Hirose, T. Anegawa, in: Proceedings on ANS topical meeting, City Park, USA, 2000.
[12] P. Portier, T. Bredel, J.-C. Brachet, V. Maillot, J.-P. Mardon, A. Lesbros, J. ASTM Int. 2(2) Paper ID JAI12468, 2005, p. 696.
[13] J. Boehnmert, Kerntechnik 57 (1992) 55.
[14] J. Bohmert, M. Dietrich, J. Linek, Nucl. Eng. Des. 147 (1993) 53.
[15] L. Yegorova, K. Liooutov, N. Jouravkova, A. Konobeev, V. Smirnov, V. Chesanov, A. Goryachev, NUREG/IA-0211, IRSn-194, NSI RRC KI 3188, US NRC, March 2005.
[16] A. Griger, L. Maroti, L. Matus, P. Windberg, in: Proceedings of Enlarged Halden Program Meeting, Leon, Norway, May 24–29, 1999.
[17] V. Asmolov, L. Yegorova, K. Lioutov, A. Konoveyev, V. Smirnov, A. Goryachev, V. Chesanov, V. Prokhorov, in: Proceedings of Nuclear Safety Research Conference, Washington DC, USA, October 28–30, 2002.
[18] L. Yegorova, K. Lioutov, in: Proceedings of Nuclear Safety Research Conference, Washington DC, USA, 20–22 October 2003.
[19] J.-C. Brachet, J. Pelchat, D. Harmon, R. Maury, P. Jacques, J.-P. Mardon, in: Proceedings of IAEA Technical Committee Meeting on Fuel Behavior Under Transient and LOCA Conditions, Halden, Norway, 10–14 September 2001.
[20] W.J. Leach, in: Proceedings of OECD Topical Meeting on LOCA Safety Criteria, Aix-en-Provence, France, 22–23 March 2001.
[21] M.H. Chung, in: Proceedings of the 2004 Int. Meeting on LWR Fuel Performance, Orlando, Florida, USA, 19–22 September 2004.
[22] J.H. Baek, K.B. Park, Y.H. Jeong, J. Nucl. Mater. 335 (2004) 443.
[23] S. Leistikow, in: Zirconium in the Nuclear Industry: Sixth International Symposium, ASTM STP 824, 1984, p. 763.
[24] L. Baker, L.C. Just, ANL-6548, 1962.
[25] J.V. Cathcart, R.E. Pawel, R.A. McKee, R.E. Druschel, G.J. Yurek, J.J. Campbell, S.H. Jury, ORNL, ORNL/NUREG-17, 1977.
[26] K. Takeda, H. Anada, in: Zirconium in the Nuclear Industry: Twelfth International Symposium, ASTM STP 1354, 2000, p. 592.
[27] J.P. Abriate, J.C. Bolcich, Bull. Alloy Phase Diagrams 3 (1) (1982) 1710.
[28] J.T. Prater, E.L. Courtright, in: Zirconium in the Nuclear Industry: Seventh International Symposium, ASTM STP 939, 1987, p. 489.
[29] R.E. Pawel, R.A. Perkins, R.A. McKee, J.V. Cathcart, G.J. Yurek, R.E. Druschel, in: Zirconium in the Nuclear Industry: Third International Symposium, ASTM STP 633, 1977, p. 199.
[30] W.G. Dobson, R.R. Biederman, R.G. Ballinger, in: Zirconium in the Nuclear Industry: Third International Symposium, ASTM STP 633, 1977, p. 150.
[31] G. Schanz, S. Leistikow, in: Proceedings of ANS/ENS Topical Meeting on Reactor Safety Aspects of Fuel Behavior, Sun Valley, Idaho, vol. 2, 2–6 August 1981, p. 342.
[32] B. Cox, J. Nucl. Mater. 29 (1969) 50.
[33] J.P. Pemsler, Electrochem. Technol. 4 (1966) 128.
[34] E. Gebhardt, H. Seghezzi, W. Durrschnabel, J. Nucl. Mater. 4 (3) (1961) 255.
[35] J.P. Abriata, J. Garces, R. Versaci, Bull. Alloy Phase Diagrams 7 (2) (1986) 116.
[36] M. Billone, Y. Yan, T. Burtseva, H. Scott, Draft NRC Report on 'Cladding Embrittlement during Postulated Loss-of-Coolant Accidents', January 2007.
[37] H.M. Chung, T.F. Kassner, NUREG/CR-1344, ANL-79-48, Argonne National Laboratory, January 1980.